2023 IEEE International Conference on Robotics and Automation (ICRA 2023)
May 29 - June 2, 2023. London, UK

Noncontact Particle Manipulation on Water Surface with Ultrasonic Phased Array System and Microscopic Vision

Yexin Zhang, Jiaqi Li, Yuyu Jia, Teng Li, Yang Wang, David C. Jeong, Hu Su*, and Song Liu*

Abstract— **Noncontact particle manipulation (NPM) shows great application potential than its conventional counterpart particularly in terms of non-invasiveness, and thus has significantly extended robotic manipulation capacity into bio-medical engineering, material science, etc. As NPM by means of electric, magnetic, and optical field has successfully demonstrated powerful strength in both academia and industry, NPM boosted by acoustic field, however, still faces staggering challenges. It is indeed in the very recent years that controllable dynamic airborne or waterborne acoustic field modulation technology emerged in academia. In this paper, we report our latest research regarding dexterous and dynamic noncontact micro-particle manipulation on water surface effected by acoustic field in terms of automated trapping, closed-loop positioning, and real-time motion planning, which can be applied to scenarios such as parallel 3D printing, cell assembly, etc. The main contribution of this work is we demonstrated the feasibility of objective-oriented and fully automated acoustic manipulation of micro-particle in precision scale based on robotic approach in 2D plane. Experiment results showed that the repetitive positioning accuracy can reach as high as 16 μm, which is essentially the pixel scale factor.**

I. Introduction

Noncontact particle manipulation (NPM) has a myriad of applications in fields such as pharmaceutical analysis [1], measurement [2], self-assembly [3], and manufacturing engineering materials [4]. In past decades, researchers and scholars worldwide have put intensive efforts into studying the possibility of using different physical fields for noncontact manipulation purposes, such as magnetic field [5] and optical field [6]. For example, the optical tweezers fostered the development of molecular biology, which makes it possible to measure DNA and protein elasticity [7]. As an emerging technology, acoustic manipulation shows great potential in broader application scenarios [8] given its advantages of excellent bio-compatibility, low power consumption, and large force output [9]. Of particular significance, acoustic waves can propagate through oblique medium and thus endows the capability of noncontact, non-invasive, and in-vivo manipulation of particles in living bodies [10]. All these merits lead to the necessity and urgency of developing next generation acoustic NPM method.

Acoustic manipulation, by working mechanism, can be categorized as static [9] versus dynamic [10], depending on whether the acoustic field can be modulated according to different working scenarios or manipulation purposes, both by utilizing acoustic radiation force [11] or acoustic streaming [12]. Static acoustic manipulation has achieved a variety of design prototypes for NPM. For example, L. Zhao *et al*. fabricated an immersive acoustic transducer encoding Fresnel lens onto bulk lead zirconate titanate (PZT) ceramic by MEMS technology to focus plane waves into a single high pressure focal point, which is capable of trapping particles up to 1 mm in diameter, like later stage zebrafish embryos [13]. X. Ding *et al*. reported standing wave tweezers of surface acoustic waves by interdigitated transducers patterned on a piezoelectric surface, which can suspend particles at pressure nodes or antinodes depending on their physical properties [14]. A. Hashmi *et al*. revealed the fact that oscillating microbubbles can produce sufficient acoustic radiation forces to trap cells, particles, or small organisms on the bubble surface by creating acoustic streaming [15]. In all, static acoustic manipulation only exhibits onefold NPM function, and thus does not support objective-setting manipulation tasks like automated particle trapping, and inherently lacks manipulation quality control.

Dynamic acoustic manipulation, from the robotic perspective, means the trapping, translating, rotating, and positioning of particles, emerging in academia in very recent years [16]. In [17-19], static acoustic tweezers were mounted onto industrial robot arm or precision motion stage, acting essentially as robot end-effector, in order to realize robotic manipulation purpose. A more compact and attractive technology supporting dynamic acoustic manipulation is by virtue of ultrasonic phased array system [20-21], which can modulate acoustic field accordingly and in real time. Though these reported works have achieved pre-loaded manipulation tasks, such as user-specified motion trajectory [22], it is still not active or control-objective oriented NPM.

In this work, taking advantage of our robotics background, we report our latest efforts towards automated NPM on water surface based on ultrasonic phased array system and microscopic vision, which could be further extended to applications such as practical parallel 3D printing, cell assembly, etc., to push forward this cutting-edge acoustic NPM technology. Rest of the paper is organized as follows: system setup and calibration are given in Section II; acoustic field design and generation method is presented in Section III. Section IV introduces control methods in trapping, positioning, and motion planning. Experiments are described in Section V.

This paper was sponsored by Shanghai Pujiang Program under Grant 21PJ1410500, and in part by the National Natural Science Foundation of China under Grant 61906191. (*Yexin Zhang and Jiaqi Li Contribute equally to this work*) (*Corresponding Author: Hu Su and Song Liu*)

Y. Zhang, J. Li, Y. Jia, T. Li, and Y. Wang are with School of Information Science and Technology, ShanghaiTech University, Shanghai 201210, China (e-mail: zhangyx5, lijq1, jiayy1, liteng1@shanghaitech.edu.cn).

D. C. Jeong is with the Department of Communication, Santa Clara University, Santa Clara, CA 95053, USA (e-mail: dcjeong@scu.edu).

H. Su is with the Institute of Automation, Chinese Academy of Sciences, Beijing 100190, China (e-mail: hu.su@ia.ac.cn).

S. Liu is with the School of Information Science and Technology, ShanghaiTech University, Shanghai 201210, China, and with Shanghai Engineering Research Center of Intelligent Vision and Imaging, Shanghai, China (e-mail: liusong@shanghaitech.edu.cn).

II. System Configuration and Calibration

A. System Configuration

The on-water-surface acoustic NPM platform, as illustrated by Fig. 1, consists of a phased transducer array (PTA) system, a microscope, and a host computer. In specific, the PTA, placed at the bottom of the water tank, is bonded to the driver board, which supplies independent multiple-channel phase-modulated sinusoidal driven voltages to PTA. A microscopic camera, which feeds back the motion status of particle on water surface is vertically mounted above the water tank. The host computer takes charge of digital image processing, and calculating the phase-only hologram (POH) to control the PTA for generating an expected acoustic field pattern per the control strategy given a certain manipulation objective. The driver board controlled by FPGAs communicates with host computer through CAN bus. In this paper, we demonstrate precision acoustic manipulation of polystyrene (PS) particle on water surface. A PS particle has positive impedance acoustic contrast against water, and would be trapped and translated by a vortex acoustic beam. A vortex acoustic beam yields vortex streaming in the propagation medium around the particle and thus induces drag force on particle to hold the particle under control [12].

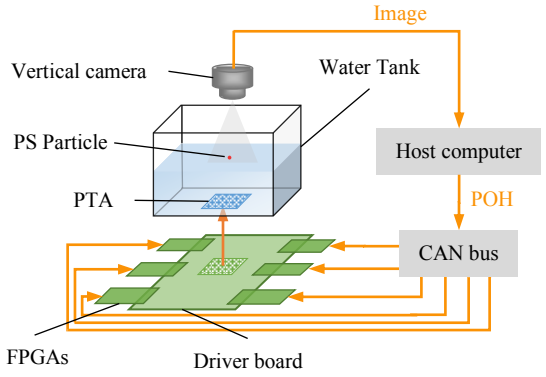

Fig. 1. Schematic diagram of the on-water-surface NPM platform, which primarily is composed of a phased array system, a microscope, and a host computer. The platform is capable of generating position-dependent vortex acoustic dream on water surface in real time, and precisely control the particle position through visual feedback.

B. Calibration

Calibration of the acoustic NPM platform concerns with the visual positioning of particle on water surface, which essentially is to determine the eye-to-hand relationship of a robot with noncontact end-effector. The coordinate systems are established as in Fig. 2. The world coordinates {**W**} is established in the water tank, with Z_W-axis perpendicular to water surface. The end-effector coordinates {**T**} is established in the top left corner of the PTA, with Z_T-axis perpendicular to PTA plane. The camera coordinates {**C**} is established on the image plane, whose X_C- and Y_C-axis have the same direction as *u*-axis and *v*-axis on the image plane.

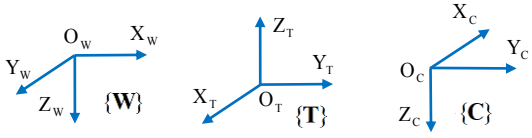

Fig. 2. Coordinate system of the acoustic NPM platform.

Acoustic vortex, as invisible robot end-effector in this case, puts challenge to eye-to-hand relationship calibration. In this paper, we propose the image Jacobian matrix-based method to solve this problem, which is defined as

$$\begin{bmatrix}\Delta u\\ \Delta v\end{bmatrix}=\begin{bmatrix}J_{11} & J_{12} & J_{13}\\ J_{21} & J_{22} & J_{23}\end{bmatrix}\begin{bmatrix}\Delta x\\ \Delta y\\ \Delta z\end{bmatrix}=\boldsymbol{J}\begin{bmatrix}\Delta x\\ \Delta y\\ \Delta z\end{bmatrix} \quad (1)$$

where Δu and Δv are motion increments in image space, Δx, Δy, and Δz are the corresponding motion increments in Cartesian space of {**T**}. For better calibration accuracy, more than three motion-increment pairs are required in the calculation with least mean square method [23].

To visualize the acoustic field, we use a needle hydrophone (Precision Acoustics Ltd., UK, tip size 200 μm) to scan the working space with a single focal point. Once the focal point is localized, the needle tip will be detected from the microscope as feature point. The scanning system is illustrated in Fig. 3, where the hydrophone is mounted on a 3-DOF motion stage. Signal from hydrophone is collected and analyzed by host computer through pre-amplifier, data acquisition (DAQ) unit, and Butterworth high-pass filter in sequence for automatic calibration purpose.

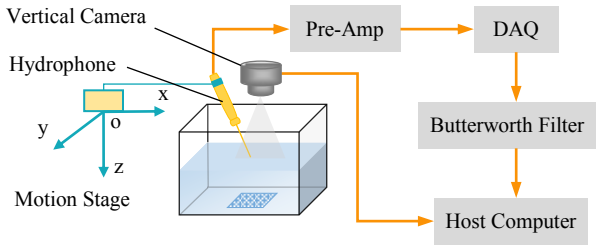

Fig. 3. Schematic of the acoustic field scanning system.

In detail, a specific position in manipulation coordinates {**T**} is labeled by a single focal point, with the corresponding POH generated from Fresnel half-wave bands (FHWB) interference method [13]. The image feature of focal point is visualized and extracted by three steps. First, generate a single-point acoustic field with known coordinate in {**T**}, and move the hydrophone to somewhere near the focal point based on the pre-determined original point in {**W**}. Afterwards, since the single focal point is in ellipsoid shape, the accurate focal position is localized by first transverse scanning in X_T-Y_T plane followed by longitudinal scanning along Z_T-axis, both seeking the pressure maximum position. Finally, move the hydrophone needle tip to the accurate location, and the corresponding image is captured. The hydrophone tip is then extracted as image feature point, together with the focal position in {**T**} to form a calibration data pair. Two calibration data pairs determine one motion-increment pair.

With more than 3 motion-increment pairs, image Jacobian matrix $\boldsymbol{J}$ can be calibrated based on least mean square method with the formula $\boldsymbol{J}=\Delta\boldsymbol{U}\Delta\boldsymbol{X}^{\boldsymbol{T}}(\Delta\boldsymbol{X}\Delta\boldsymbol{X}^{\boldsymbol{T}})^{-1}$, where $\Delta\boldsymbol{U}$ is the matrix formed by motion increments in image space and $\Delta\boldsymbol{X}$ is the matrix formed by the corresponding motion increments in {**T**}. Once $\boldsymbol{J}$ is calibrated, one PS particle on water surface can be localized in {**T**}, by referring to calibration data pair and the particle's geometrical center in image, as

$$\begin{bmatrix} x_p \\ y_p \\ z_p \end{bmatrix}_T = \boldsymbol{J}^{\dagger}\left(\begin{bmatrix} u \\ v \end{bmatrix} - \begin{bmatrix} u_{avg} \\ v_{avg} \end{bmatrix}\right) + \begin{bmatrix} x_{avg} \\ y_{avg} \\ z_{avg} \end{bmatrix} \quad (2)$$

where subscript *avg* refers to average coordinates of the calibration data pairs. Since Eq. 2 is underdetermined, z_p is set manually to be the water surface altitude in {**T**}.

III. Acoustic Field Design and Simulation

A. Acoustic Field Design Methodology

A particle with positive impedance contrast against propagation medium can be trapped by a vortex beam [21]. The most well-known vortex beam generation method through PTA is the iterative backpropagation (IB) method proposed in [16], which is substantially a revised version of interactive angular spectrum approach (IASA) [24]. However, IB method is inherently time-consuming, particularly given larger PTA size and control points number, thus is unsuitable for real-time acoustic manipulation scenarios. In this paper, we propose a novel acoustic vortex beam generation method with excellent real-time performance for PTA. In specific, as shown in Fig. 4, the vortex beam is designed by nine control points centered around a target position in {**T**}, with phase dislocation increasing evenly from 0 to 2π. The vortex size is modulated by changing the distance between the target point and nine control points. Correspondingly, the PTA channels are grouped into 3 × 3 sized sub-blocks, with each channel in every sub-block assigned to be responsible for one specific control point. For every single control point, FHWB method is used to calculate corresponding channel phase on the PTA by

$$\theta(\vec{\boldsymbol{x}}) = 2\pi - \mathrm{mod}\left(-\frac{2\pi}{\lambda}\| \vec{\boldsymbol{x}} - \vec{\boldsymbol{x}}_c \|_2, 2\pi\right) + \frac{\boldsymbol{i}}{9}2\pi \quad (3)$$

where $\vec{\boldsymbol{x}}$ is the channel coordinate, $\vec{\boldsymbol{x}}_c$ is the control point coordinate in {**T**}, and i is the control point index in circular sequence to control phase dislocation.

The proposed real-time acoustic vortex generation method for PTA applies the concept of spatial multiplexing by virtue of the PTA's high density and high spatial-bandwidth in this work. It is validated to be effective by both simulation and experiments with 50 × 50 PTA. For PTA with less channels, the proposed method may be not applicable.

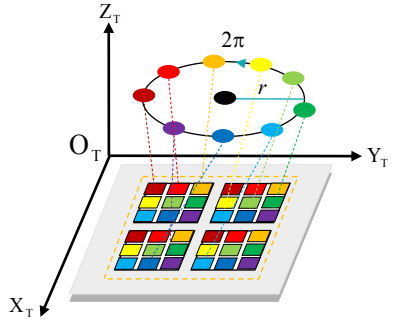

Fig. 4. Schematic of generating acoustic vortex for PTA through nine control points with phase dislocation increasing evenly from 0 to 2π. The r is the vortex radius controlling vortex size, which is determined upon particle dimension. The PTA channels are grouped into 3×3 sized sub-blocks, with each channel in every sub-block assigned to be responsible for one specific control point. The color depicts the assignments.

B. Simulation Results

In order to validate the effectiveness of the proposed real-time acoustic vortex generation method, simulation works with Python 3.10.6 and angular spectrum method (ASM) [25] are conducted. Fig. 5 shows the simulation results. The vortex is centered at $[25, 25, 53]^T$ mm in {**T**} with radius of 1.2 mm. The PTA in simulation is in size of 50 × 50 with pitch of 1 mm, working at 2.3 MHz. Sound velocity is 1480 m/s. As can be seen, the vortex exhibits circular pressure profile and periodic phase dislocation at transverse plane of target altitude, which conforms to an ideal acoustic vortex.

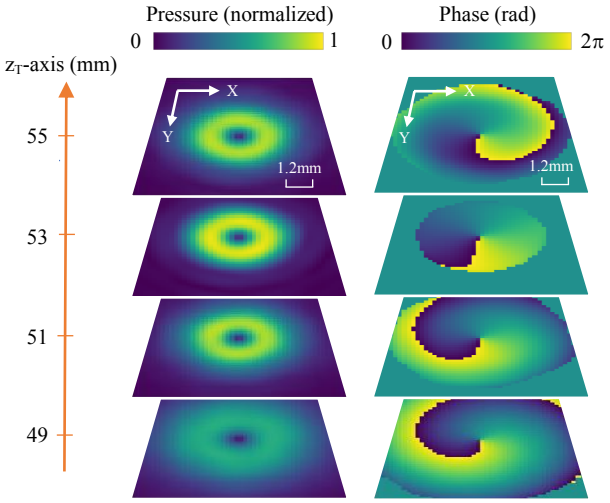

Fig. 5. Simulation results of an acoustic vortex at $[25, 25, 53]^T$ mm in {**T**} with transverse pressure and phase profile at different altitudes along the z_T-axis. The diameter is 2.4 mm.

IV. Auto Trapping, Positioning, and Motion Planning

A. Feature Extraction and Particle Localization

For real-time position-based visual servo control, the primary consideration is extracting features from image so that the object can be localized accurately. In this work, extraction of the geometrical center of PS particle in image follows four-step procedure. To start with, do background subtraction to the image grabbed from the microscope. Region of interest (ROI) is localized by template matching based on the foreknown particle size. Then, apply thresholding and morphological operations to ROI to filter noises. Afterwards, find out the particle's contours and sift the target according to the contour area. Finally, the geometrical coordinate of particle in image is obtained by fitting the pixels on the contour into ellipse by RANSAC. The particle position in 3D space is then computed through Eq. 2. This method is particularly effective considering the small particle size compared against the large field of view (FOV) of microscope. The extracted feature coordinates are expressed in sub-pixel resolution so that the localization and manipulation accuracy is further improved.

B. Automated Trapping of PS Particle

Particles on still water surface exhibit simple motion status, either keeping static or floating around freely and slowly. However, automated trapping of particle, though not the focus of this paper, is fundamental for further advanced manipulation to avoid manual interference, regardless the

particle motion status. Automated trapping of PS particle on water surface is realized by our method in [26]. In general, after releasing the PS particle on the water surface without any position constraint, an acoustic vortex will be generated at the particle position per the feedback from microscope, trapping the particle firmly. The vortex radius is determined upon on the particle size under manipulation.

C. Particle Positioning with Visual Feedback

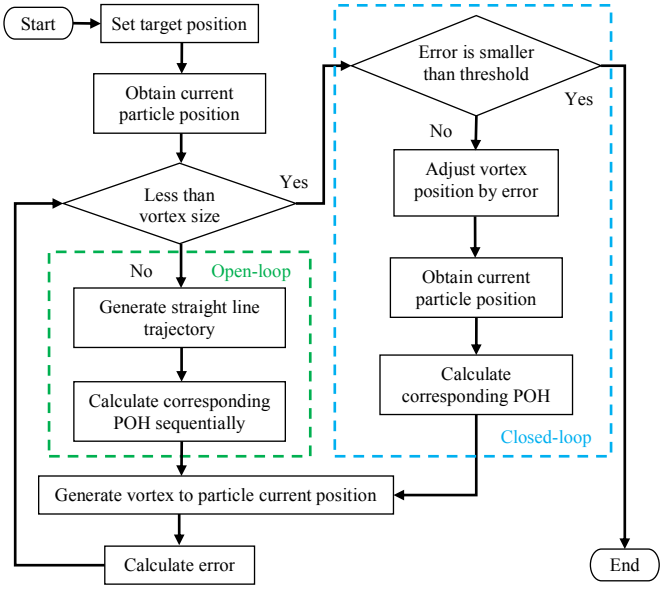

Fig. 6. Particle positioning control strategy, including open-loop followed by closed-loop control.

Particle positioning concerns with moving a trapped particle to a specific position for certain application purpose through actively controlling acoustic field, like conventional positioning of robot end-effector in working space. Therefore, particle positioning is objective-oriented manipulation with necessary closed-loop control for better precision. In this work, a PS particle at an arbitrary place in working space will be precisely and automatically translated to a target position after being trapped. The particle positioning control strategy is composed of two stages, i.e., open-loop control and closed-loop control, as depicted in Fig. 6. The open-loop control aims at moving the particle rapidly towards somewhere near the target position, along a straight line. In specific, a straight-line trajectory, starting from initial particle position to target position, is generated by dividing the distance against step size. Then, the POHs for each intermediate position along the trajectory are calculated per the method given in Section III.A. Then vortex beams are generated on the water surface sequentially with constant updating frequency, stably translating the particle to the target point. Finally, open-loop control finishes once the error between the target point and the current particle position is less than vortex radius. The step size and updating frequency determine the particle translation velocity. Typically, step size is set to be less than vortex radius, while acoustic field updating frequency is determined by trial and error. Larger step size or higher updating frequency probably results in losing of particle during translation process, causing instability problem, which is closely related to particle size.

The closed-loop control is necessary because vortex position does not always align well to particle position under trapping status. Therefore, the vortex position is adjusted by the misalignment error between particle position and target position. Essentially, the closed-loop control strategy used is integral controller, updating the vortex position by

$$\vec{\boldsymbol{x}}_{n+1} = \vec{\boldsymbol{x}}_n + \boldsymbol{K}_{ip}\Delta\vec{\boldsymbol{e}}_n \tag{4}$$

where $\vec{\boldsymbol{x}}_n$ is current vortex position, and $\Delta\vec{\boldsymbol{e}}_n$ is the position misalignment error calculated by Eq. 2, n is the control loop index, and K_{ip} is integral coefficient for positioning.

D. Motion Planning

Particle motion planning is essentially crucial in applications like moving a specific sample out of complicated sample cluster for further analysis. Therefore, it is highly control objective oriented, and thus user-specified trajectory planning is not suitable. Motion planning should substantially apply double closed-loop structure, considering the disparity between vortex position and particle position, with the control objective of making the particle follow the planned trajectory more tightly. This section presents a feasible visual servo integral controller as inner-loop control for particle motion planning, as

$$\left(\vec{\boldsymbol{x}}_m\right)_a = \left(\vec{\boldsymbol{x}}_m\right)_p + \boldsymbol{K}_{it}\sum_{n=1}^{m-1}\Delta\vec{\boldsymbol{e}}_n \tag{5}$$

where $(\vec{\boldsymbol{x}}_m)_p$ is planned vortex position, $(\vec{\boldsymbol{x}}_m)_a$ is adjusted vortex position, m is the point index in planned trajectory, and K_{it} is integral coefficient for motion planning. The basic design philosophy of this controller is we assume the disparity between vortex position and particle position is systematic error, which can be compensated by adding a bias to control variable. Both the integral parameter K_{ip} and K_{it} are set by trial and error.

V. Experiments and Results

A. Experimental System Setup

The acoustic NPM platform described in Section II-A is physically prototyped as demonstrated in Fig. 7 (a). Regarding the phased array system, the PTA with 50 × 50 channels is fabricated on 1 mm thick bulk lead zirconate titanate (PZT) ceramic by photo lithography and wet etching with nickel electrode on both sides. Transducer size of each channel is 800 × 800 μm, with transducer pitch of 1 mm. The driver board consists of six FPGAs working at 400 MHz in master-slave structure. The CAN-Bus controller works at baud rate of 500 kbps, enabling POH updating at 11 frames per second (FPS). The microscope employed has Prosilica GC2450 microscopic cameras, equipped with Navitar zoom lens, capable of capturing images in 15 FPS by size of 2448 ×2050. FOV of the microscope is about 30 × 35 mm.

We first validated the functionality of the acoustic NPM platform in generating acoustic vortex. Fig. 7 (b) shows the scanned transverse acoustic pressure profiles at different altitudes with the same parameters used in simulation in Section III.B. The acoustic NPM platform generated a vortex at the target position, conforming simulation results in Fig. 5.

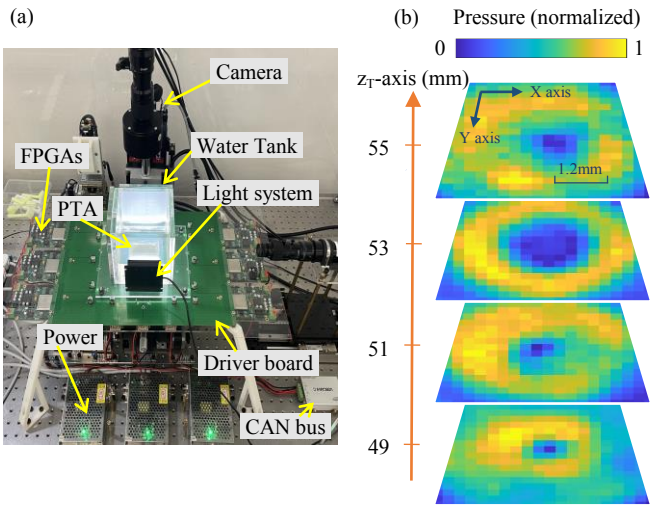

Fig. 7. The established acoustic NPM platform with characterized vortex beam. (a) The acoustic NPM platform. (b) The scanned transverse pressure profiles of the vortex at $[25, 25, 53]^T$ mm in $\{\mathbf{T}\}$ generated by the acoustic NPM platform. Vortex diameter is designed to be 2.4 mm.

B. Calibration Results

By the calibration procedure presented in Section II.B, 12 calibration data pairs were obtained to generate 24 motion-increment pairs for image Jacobian matrix calculation,

$$\boldsymbol{J} = \begin{bmatrix} -0.063463 & -0.004537 & -0.000158 \\ 0.004172 & -0.063862 & 0.001618 \end{bmatrix}. \quad (6)$$

The centroid of the calibration data pairs were $[u_{avg}, v_{agv}]^T = [1330.00, 723.25]^T$ pixel and $[x_{avg}, y_{avg}, z_{avg}]^T = [25.00, 25.00, 46.33]^T$ mm. The particle localization error is evaluated by comparing checkpoint's coordinate in $\{\mathbf{T}\}$ and the one estimated by Eq. 2. The result reveals that all errors are less than 180 µm, and the average is 39 µm, much smaller than the diameter of the PS particle used in this work. Hence, this calibration result is accurate enough to localize the particle and realize precision particle manipulation in micron-level.

C. Auto Trapping Experiments

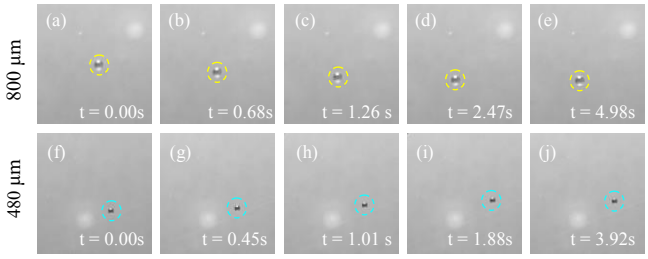

Fig. 8. The automated trapping trajectories of the PS particles. (a)-(e) was the trapping trajectory of the particle with 800 µm diameter. From 0.00 s to 1.26s, the particle freely floated around on the water surface. Since 2.47s, the particle was trapped and stayed still after then. (f)-(j) is the trapping trajectory of the particle with 480 µm diameter. From 0.00s to 1.01s, the particle freely floated around on the water surface. Since 1.88s, the particle was trapped and stayed still after then.

PS particles, with size of 480 µm and 800 µm in diameter, were chosen for auto trapping experiments. Different vortex radii were tested to select the most suitable vortex size. By experiments, 600 µm vortex is best for 480 µm diameter PS particle trapping and 900 µm vortex for 800 µm diameter PS particle in terms of trapping stability. Fig. 8 shows the trapping process of free-floating PS particles.

D. Positioning Experiments

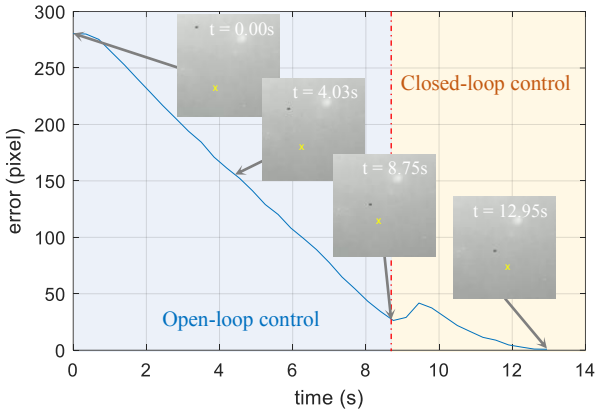

Fig. 9. The error curve of positioning a 480 µm diameter PS particle to the target position, using acoustic vortex with diameter of 600 µm. The integral coefficient is 0.2, the step size is 0.56 times the vortex radius, and POH updating frequency is 3 Hz.

TABLE I. REPETITIVE POSITIONING EXPERIMENT RESULTS WITH DIFFERENT PARTICLE SIZES

No.	Particle size (µm)	Performance		
		Open-loop error (pixel)	Closed-loop error (pixel)	Step number
1	480	26.3339	0.8421	13
2		26.7888	0.6282	15
3		28.9991	0.8701	14
4		34.2802	0.7382	12
5		32.6860	0.6389	16
Average value		29.8176	0.7435	14
6	800	19.8803	0.8026	13
7		20.6426	0.5608	14
8		16.9361	0.9708	13
9		20.7165	0.9841	14
10		25.0363	0.1118	14
Average value		20.6424	0.6860	13.6

The positioning experiment was also conducted over 480 µm and 800 µm diameter PS particles. The integral coefficient K_{ip} was determined to be 0.2 by experiments, and the termination condition was less than 1 pixel (or 16 µm). The positioning process of 480 µm diameter PS particle is given in Fig. 9. In open-loop control stage, the position error decreased linearly until a short distance was left between the particle position and the target position. Then, closed-loop control started, with the position error continuously decreasing until reaching our expectation.

The repetitive experiment results were given in Table I. For 480 µm diameter PS particles, the step size was 0.56 times vortex radius with 3 Hz updating frequency. The final positioning error can reach as small as 0.6282 pixels (approximately 10.05µm). For 800 µm diameter PS particle, the step size is 0.48 times the vortex radius with 3 Hz updating frequency. The final error can reach as small as 0.6118 pixels (approximately 9.79µm). On average, closed-loop control converged in about 14 control steps.

E. Motion Planning Experiments

Compared with linear motion trajectory, a circular trajectory is more challenging and superior to demonstrate the performance of the closed-loop visual servo controller in Eq. 5. Therefore, a circular trajectory with radius of 250 pixels in image plane was generated in advance, as depicted in Fig. 9, labeled 'plan trajectory'. For the control group, acoustic vortex was generated sequentially, and the particle motion trajectory in image was recorded (Fig. 12 (a)). Then, the closed-loop control strategy was applied to the system, and the particle motion trajectory was demonstrated in Fig. 10. (b). As can be seen that position errors along the trajectory with closed-loop control outperform that of open-loop control.

Repetitive motion planning experiments were also conducted over 480 μm and 800 μm diameter PS particles, as listed in Table II. The average positioning error was about 100 μm. Compared with motion trajectory with open-loop control, the average position error and standard deviation of position errors with closed-loop control were significantly decreased by 74.8% and 57.2% for 480 μm diameter PS particle case, and 72.0% and 58.8% for 800 μm diameter PS particle case. All experiment results well demonstrate the precision manipulation capability of robotic acoustic NPM technology. With a more sophisticated motion planning control strategy, the position errors along trajectory can be further decreased.

For reader clarity and interest, we moved 480 μm diameter PS particle along the trajectory of four letters 'A', 'M,' 'N,' and 'R,' standing for Acoustic Manipulation Nano Robot. Fig. 10 shows the superimposed trajectory of the particle.

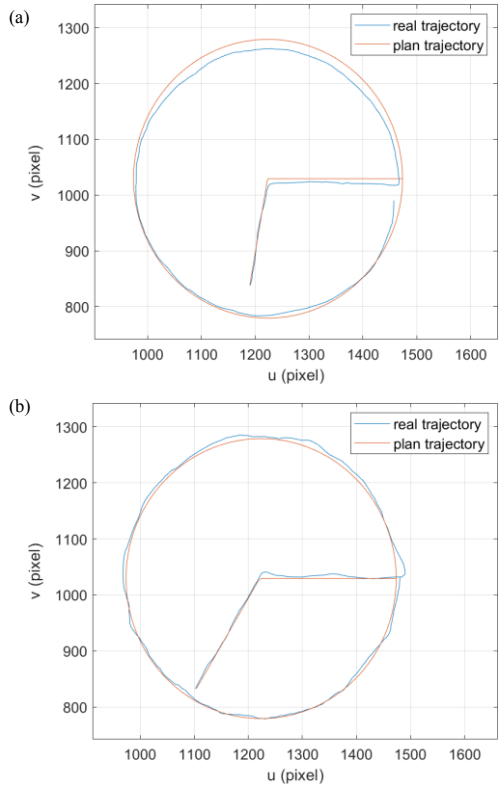

Fig. 9. Comparative experiment results regarding motion planning with (a) and without (b) visual feedback over 480 μm diameter PS particle. The integral coefficient is set to 0.22, the step size is 0.56 times the vortex radius, and POH updating frequency is 3 Hz.

TABLE II. REPETITIVE MOTION PLANNING EXPERIEMNT RESULTS WITH DIFFERENT PARTICLE SIZES

No.	Particle size (μm)	Error	
		Average (pixel)	Standard deviation
ref	480	28.4140	10.7867
1		5.4621	3.2019
2		5.8469	3.9893
3		6.9772	4.7499
4		9.2341	6.0233
5		8.3232	5.0957
Average value		7.1687	4.6120
ref	800	19.3305	7.2347
6		5.3322	2.7288
7		5.4653	3.0246
8		5.3226	3.0236
9		5.2731	2.9003
10		5.6329	3.2418
Average value		5.4052	2.9838

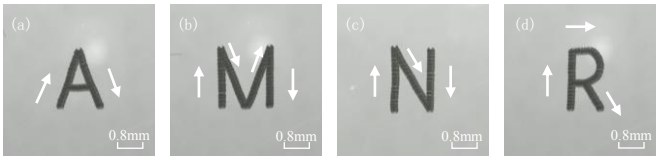

Fig. 10. The superimposed trajectory of 480 μm diameter PS particle along the four letters of 'A', 'M', 'N', 'R'. Video is available from https://www.amnrlab.org/research.

VI. CONCLUSION

The main contribution of this work is, for the first time, we testified the feasibility of precision acoustic manipulation over micro-particle in micron-scale by applying robotic approach, in terms of auto trapping, automated positioning, and motion planning. Experiments show that the positioning accuracy can reach as high as 16 μm with the proposed integral controller. Besides, position errors in translating a particle along a desired trajectory are less than a quarter of the smallest particle diameter in average. We also proposed a novel vortex beam generating method, i.e., spatial multiplexing, for PTA with real-time performance, which enables closed-loop visual feedback control for acoustic NPM. We anticipate that precision robotic acoustic manipulation exhibits great potential for numerous applications in various fields. Our future works will focus on developing sophisticated and more robust control strategies for robotic acoustic NPM, and apply the technology to biomedical engineering, like single-cell analysis, etc.

REFERENCES

[1] S. Santesson, and S. Nilsson, "Airborne chemistry: acoustic levitation in chemical analysis," *Analytical and Bioanalytical Chemistry*, vol. 378, no. 7, pp. 1704-1709, 2004.

[2] T. Li, S. Kheifets, D. Medellin, and M. G. Raizen, "Measurement of the instantaneous velocity of a Brownian particle," *Science*, vol. 328, no. 5986, pp. 1673–1675, 2010.

[3] M. Prisbrey, J. Greenhall, F. G. Vasquez, and B. Raeymaekers, "Ultrasound directed self-assembly of three-dimensional user-specified patterns of particles in a fluid medium," *Journal of Applied Physics*, vol. 121, no. 1, pp. 014302:1-6, 2017.

[4] Z. Ma, A. W. Holle, K. Melde, T. Qiu, K. Poeppel, V. M. Kadiri, and P. Fischer, "Acoustic holographic cell patterning in a bio-compatible hydrogel," *Advanced Materials*, vol. 32, no. 4, pp. 1904181:1-6, 2020.

[5] S. H. Kim, and K. Ishiyama, "Magnetic robot and manipulation for active-locomotion with targeted drug release", *IEEE Transactions on Mechatronics*, vol. 19, no. 5, pp. 1651-1659, 2014.

[6] M. Z. Miskin, A. J. Cortese, K. Dorsey, et al, "Electronically integrated, mass-manufactured, microscopic Robots", *Nature*, vol. 584, no. 7822, pp. 557-561, 2020.

[7] M. D. Wang, H. Yin, R. Landick, J. Gelles, and S. M. Block, "Stretching DNA with optical tweezers", *Biophysical Journal*, vol. 72, no. 3, pp. 1335-1346, 1997.

[8] A. Ozcelik, J. Rufo, F. Guo, Y. Gu, P. Li, et al, "Acoustic tweezers for the lift sciences", *Nature Methods*, vol. 15, no. 12, pp. 1021-1028, 2018.

[9] Y. Tang, S. Liu, and E. S. Kim, "MEMS focused ultrasonics transducer with air-cavity lens based on polydimethylsiloxane (PDMS) membrane", *the 33rd IEEE International Conference on Micro Electromechanical Systems*, pp. 58-61, 2020.

[10] M. A. Ghanem, A. D. Maxwell, Y. N. Wang, B. W. Cunitz, V. A. Khokhlova, O. A. Sapozhnikov and M.R. Bailey, "Noninvasive acoustic manipulation of objects in a living body," *Proceedings of the National Academy of Sciences* (*PNAS*), vol. 117, no. 29, pp, 16848-16855, Jul. 2020.

[11] A. Marzo, S. A. Seah, B. W. Drinkwater, D. R. Sahoo, B. Long, and S. Subramanian, "Holographic acoustic elements for manipulation of levitated objects," *Nature Communication*, 6:8661, 2015.

[12] J. Rufo, F. Cai, J. Friend, M. Wiklund, and T. J. Huang, "Acoustofluidics for biomedical applications," *Nature Review Methods Primers*, 2:30, 2022.

[13] L. Zhao and E.S. Kim, "Acoustic Tweezers for Trapping Late-Stage Zebrafish Embryos," *IEEE International Conference on Micro Electro Mechanical Systems*, pp. 57– 60, 2019.

[14] X. Ding, P. Li, S. C. Lin, Z. S. Stratton, N. Nama, F. Guo, D. Slotcavage, X. Mao, J. Shi, F. Costanzo, and T. J. Huang, "Surface acoustic wave microfluidics," *Lab on a Chip,* vol. 13, no. 18, pp. 3626-3649, 2013.

[15] A. Hashmi, G. Y, M. R. Collette, G. Heiman, and J. Xu, "Oscillating bubbles: a versatile tool for lab on a chip application," *Lab on a Chip*, vol. 12, no. 21, pp. 4216-4227, 2012.

[16] A. Marzo, and B. W. Drinkwater, "Holographic Acoustic Tweezers", *Proceedings of the National Academy of Sciences*, vol. 116, no. 1, pp. 84-89, 2019.

[17] J. Nakahara, B. Yang, and J. R. Smith, "Contactless manipulation of millimeter-scale objects via ultrasonic levitation," *IEEE RAS/EMBS International Conference for Biomedical Robotics and Biomechatronics*, pp. 264-271, 2020.

[18] M. Baudoin, J. L. Thomas, R. A. Sahely, J. C. Gerbedoen, Z. Gong, A. Sivery, O. B. Matar, N. Smagin, P. Favreau, and A. Vlandas. "Spatially selective manipulation of cells with single-beam acoustical tweezers," *Nature communications*, vol. 11, no. 1, pp. 1-10, 2020.

[19] X. Guo, Z. Ma, R. Goyal, M. Jeong, W. Pang, P. Fischer, X. Duan, and T. Qiu, "Acoustofluidic tweezers for the 3D manipulation of microparticles," *IEEE International Conference on Robotics and Automation*, pp. 11392-11397, 2020.

[20] R. Morris, E. R. Dye, P. Docker, and M. Newton, "Beyond the Langevin horn: transducer array for the acoustic levitation of liquid drops," *Physics of Fluids*, vol. 31, no. 10, pp. 101301:1-10, 2019.

[21] Y. Yang, T. Ma, Q. Zhang, J. Huang, Q. Hu, Y. Li, C. Wang, and H. Zheng, "3D acoustic manipulation of living cells and organisms based on 2D array," *IEEE Transactions on Biomedical Engineering*, vol. 69, no. 7, pp. 2342-2352, 2022.

[22] M. Prisbrey, and B. Raeymaekers, "Ultrasound noncontact particle manipulation of three-dimensional dynamic user-specified patterns of particles in air," *Physical Review Applied*, vol. 10, no. 3, pp. 034066:1-9, 2018.

[23] S. Liu, D. Xu, D. Zhang, and Z. Zhang, "High Precision Automatic Assembly Based on Microscopic Vision and Force Information", *IEEE Transactions on Automation Science and Engineering*, vol. 13, no. 1, pp. 382–393, 2016.

[24] C. Zhong, Y. Jia, D. C. Jeong, Y. Guo, S. Liu, "AcousNet: A Deep Learning based Approach to Dynamic 3D Holographic Acoustic Field Generation from Phased Transducer Array", *IEEE Robotics and Automation Letters*, vol. 7, no. 2, pp. 666-673, 2021.

[25] C. Zhong, Z. Sun, K. Lv, Y. Guo, and S. Liu, "Real-time Acoustic Holography with Physics-based Deep Learning for Acoustic Robot Manipulation", *IEEE International Conference on Intelligent Robots and Systems*, Kyoto, Japan, Oct. 23-27, 2022.

[26] M. Wang, J. Li, Y. Jia, Z. Sun, Y. Liu, T. Li, and S. Liu, "Automated Noncontact Trapping of Moving Micro-particle with Ultrasonic Phased Array System and Microscopic Vision", *arXiv*:2208.10409, 2022.